Macromolecules
ARTICLE

Macromolecules **2010**, *43*, 4761–4770 **4761**
DOI: 10.1021/ma100609k

Crystallization in Ordered Polydisperse Polyolefin Diblock Copolymers

Sheng Li and Richard A. Register*

Department of Chemical Engineering, Princeton University, Princeton, New Jersey 08544

Brian G. Landes, Phillip D. Hustad, and Jeffrey D. Weinhold

The Dow Chemical Company, Core R&D, Midland, Michigan 48674, and Freeport, Texas 77541

Received March 19, 2010; Revised Manuscript Received April 21, 2010

ABSTRACT: The morphologies of polydisperse ethylene−octene diblock copolymers, synthesized via a novel coordinative chain transfer polymerization process, are examined using two-dimensional synchrotron small-angle and wide-angle X-ray scattering on flow-aligned specimens. The diblock copolymers comprise one amorphous block with high 1-octene content and one semicrystalline block with relatively low 1-octene content, and each block ideally exhibits the most-probable distribution. Near-symmetric diblocks with a sufficiently large octene differential between the amorphous and semicrystalline blocks show well-ordered lamellar domain structures with long periods exceeding 100 nm. Orientation of these domain structures persists through multiple melting/recrystallization cycles, reflecting a robust structure which self-assembles in the melt. The domain spacings are nearly 3-fold larger than those in near-monodisperse polyethylene block copolymers of similar molecular weights. Although the well-ordered lamellar domain structure established in the melt is preserved in the solid state, the crystallites are isotropic in orientation. These materials display crystallization kinetics consistent with a spreading growth habit, indicating that the lamellae do not confine or template the growing crystals. The exceptionally large domain spacings and isotropic crystal growth are attributed to interblock mixing resulting from the large polydispersity; short hard blocks dissolved in the soft-block-rich domains swell the domain spacing in the melt and allow hard block crystallization to proceed across the lamellar domain interfaces.

Introduction

In semicrystalline block copolymers, the formation of solid-state structure can be driven either by block incompatibility or by crystallization of one or more blocks.[1−3] Depending on the block interaction strength, represented by the quantity χN, where χ is the Flory−Huggins interaction parameter and N is the degree of polymerization, a wide array of solid-state morphologies may be observed. When the value of χN is small, the dissimilar blocks are mixed in the melt; crystallization then leads to a solid-state structure of alternating crystalline/amorphous lamellae exhibiting a spherulitic superstructure, regardless of the copolymer composition.[4,5] When χN is larger and the melt is microphase-separated, then depending on the block segregation strength, different morphologies including breakout, templated, and confined crystallizations may be observed.[6,7] "Breakout" describes the scenario where a microphase-separated morphology is destroyed by crystal growth and replaced by an alternating lamellar structure and spherulitic superstructure much like those which form from a homogeneous melt. Breakout typically occurs when the melt is weakly segregated.[8−11] At higher values of χN, the ordered melt morphology is largely retained in the solid state and can be further divided into two types, depending on the morphology and the segregation strength: "confined" crystallization,[12] where no crystals bridge between crystallizable microdomains and each microdomain must be individually nucleated, and "templated" crystallization,[13−15] where occasional bridging events permit multiple microdomains to be crystallized from a single nucleus, greatly accelerating the crystallization kinetics while preserving the overall microdomain structure established in the melt. Templated and confined crystallizations also affect crystal orientation; most commonly, the fast growth direction of the crystals is aligned with the long axis of the microdomain to allow unfettered growth in that direction.[16−19]

In this work, we explore both the melt and solid-state morphologies of polydisperse ethylene−octene semicrystalline diblock copolymers, consisting of one crystallizable "hard" block of low 1-octene content and one noncrystallizable "soft" block of high 1-octene content, synthesized by a coordinative chain transfer polymerization recently developed at Dow Chemical.[20] When the difference in octene content between hard and soft blocks (i.e., χ) and the block molecular weight (i.e., N) are sufficiently high, the block copolymers exhibit suppressed spherulite growth and unusual optical properties, appearing blue in reflection and yellow in transmission.[21] These observations suggest confined or templated crystallization from an ordered melt, where the domain periodicity exceeds 100 nm; transmission electron microscopy on selected diblocks has indeed revealed such large-period lamellae, though with a high density of defects.[21]

Because the diblocks are prepared in two cascaded continuous-flow stirred reactors, each block ideally exhibits the most probable distribution of chain lengths.[20,21] This provides an excellent opportunity to investigate the effect of polydispersity on morphology, particularly in the weakly segregated regime. The influence of polydispersity on block copolymer self-assembly has received increasing attention in recent years.[22] Increasing a block copolymer's polydispersity is theoretically predicted to both stabilize the ordered microphases and increase their domain periodicities.[23−27] Experimental studies in this area, although limited, are generally in qualitative agreement with the theoretical

*Corresponding author. E-mail: register@princeton.edu.

Published on Web 04/28/2010

Table 1. Process Conditions for Synthesis of High-Octene Diblocks

	CSTR 1[a]			CSTR 2[b]						
sample code	cat (g/h)	cocat (g/h)	conv[c] (%)	solv (kg/h)	C_2H_4 (kg/h)	C_8H_{16} (kg/h)	cat (g/h)	cocat (g/h)	MMAO (g/h)	conv[c] (%)
H69	210	240	92	12.0	0.55	4.5	90	77	100	89
H81	180	210	90	14.0	0.64	4.1	75	89	100	89
H89	170	200	91	14.0	0.40	5.3	62	74	97	91
H93	165	198	90	14.0	0.55	4.5	65	78	100	91

[a] General conditions for CSTR 1: solvent flow = 14 kg/h, ethylene feed = 1.44 kg/h, 1-octene feed = 0.38 kg/h, T = 120 °C, catalyst feed concentration = 89 ppm of Hf, cocatalyst feed concentration = 600 ppm, CSA feed concentration = 10 000 ppm Zn, CSA feed = 98 g/h. [b] General conditions for CSTR 2: T = 120 °C, catalyst feed concentration = 89 ppm of Hf, cocatalyst feed concentration = 600 ppm, MMAO (modified methylaluminoxane) feed concentration = 98 ppm Al. [c] Conversion = percent ethylene conversion.

Table 2. Polyolefin Diblock Copolymer Characterization Data

sample code	C8 in hard block (mol %)	C8 in soft block (mol %)	f_{hard} (wt %)	M_n (kg/mol)	PDI	$T_{m,peak}$[a] (°C)	$T_{c,onset}$[b] (°C)	w_c[a]	χN[c] at T = 167 °C	d_{DS} (nm)
H69	4.8	35.3	50.4	69	2.16	99	80	0.27	6	128
H81	4.7	30.4	51.6	81	1.92	103	85	0.30	6	128
H89	4.5	42.8	47.8	89	1.90	99	81	0.30	10	145
H93	4.9	35.5	48.0	93	2.09	100	84	0.30	8	158
L52	0.5	10.8	31.0	52	1.67	122	105	0.72	2	

[a] Heating at 10 °C/min. [b] Cooling at 10 °C/min. [c] Calculated by weight-fraction extrapolation of solubility parameter data (eq 5).

predictions.[28−34] However, since it is nontrivial to precisely tune the molecular weight distribution of a polymer during synthesis, many early experimental studies blended monodisperse block copolymers of different molecular weights or compositions to generate polydispersity.[28−30] Although straightforward to prepare, such blends are likely to differ in their behavior from copolymers with continuous molecular weight distributions due to the inherent correlations between the lengths of the two blocks in a given chain. More recently, Hillmyer et al. have synthesized block copolymers containing one polydisperse and one near-monodisperse block and characterized their phase behavior.[31−34] The olefin diblock copolymers studied here, which have two polydisperse blocks with known and uncorrelated distributions, take this idea a step further: as shown below, the domain periodicities exhibited by these polydisperse olefin diblock copolymers are several times larger than those exhibited by monodisperse block copolymers of similar chemical structures and molecular weights. Yet surprisingly, these domains exert negligible influence on the orientation of growing polyethylene crystals—another consequence of extensive interblock mixing in these polydisperse diblocks.

Experimental Section

Materials. The polymerization reaction was carried out in two continuous stirred tank reactors (CSTRs) arranged in series, in a process described previously,[20,21] using a Hf-based catalyst and diethylzinc as the chain shuttling agent (CSA). Briefly, monomers, solvent, and catalyst components were fed to each reactor, so that by independent control of the conditions in each reactor, the chain length and octene content of the hard and soft blocks could be independently controlled. The "hard" (low octene) block was synthesized in the first reactor and the "soft" (high octene) block added in the second, with the final polymers converted to pellet form. Four "high octene" diblocks were synthesized, each with > 30 mol % (> 63 wt %) 1-octene in the soft block. Each high-octene diblock is identified by the code "H*xy*", where "H" reflects the high octene content and "*xy*" indicates the polymer's true number-average molecular weight, M_n, in kg/mol. Specific process conditions for the synthesis of each of the high-octene diblocks are given in Table 1; the synthesis of diblock H93 has been described previously.[21] In addition to the high-octene diblock copolymers, one diblock copolymer with relatively low octene content was also examined, whose synthesis was also reported previously;[20] this polymer is here designated L52.

Relevant characteristics of the five diblocks examined are shown in Table 2. The total octene content, as well as the octene content in the hard block, was measured by ^{13}C NMR. The octene content in the soft block was determined by ^{1}H NMR on material extracted from the pellets by stirring in *n*-hexane at room temperature for 10 days, subsequently confirmed by ^{13}C NMR on the same extracts. The relative block lengths, given as wt % hard block, f_{hard}, were calculated based on the three measured octene contents for each diblock. The molecular weight distribution of each polymer was measured by high-temperature gel permeation chromatography (GPC) in 1,2,4-trichlorobenzene at 140 °C, relative to linear polyethylenes of the same elution time, thus yielding "polyethylene-equivalent" molecular weights, M_{PEeqv}. These apparent molecular weights were converted to best estimates of the true values according to[35,36]

$$M = \frac{M_{PEeqv}}{1 + w_{oct}^{tot}(r_{oct} - 1)} \quad (1)$$

where w_{oct}^{tot} is the measured total octene content. The hydrodynamic equivalence ratio for polyoctene, r_{oct}, is defined as

$$r_{oct} = \frac{M_{PEeqv,polyoctene}}{M_{polyoctene}} \quad (2)$$

r_{oct} was estimated as 0.37, using eq 1 and absolute molecular weight values for diblocks H69 and H93 determined by online light scattering during GPC. Apparent polydispersity indices (PDI = M_w/M_n, where M_w is the weight-average molecular weight) were calculated directly from the polyethylene-equivalent values.

Measurements. Differential scanning calorimetry (DSC) measurements employed a Perkin-Elmer DSC 7 equipped with an intracooler and calibrated with indium and tin. 5−10 mg specimens of each polymer were cut from the as-received pellets, heated to 160 °C, cooled to 10 at 10 °C/min, held for 15 min, and then reheated to 160 at 10 °C/min. The peak melting temperature, $T_{m,peak}$, and heat of melting, ΔH_m, of each diblock copolymer were obtained during the reheating ramp (i.e., on the second heat), while the onset crystallization temperature, $T_{c,onset}$, was obtained from the cooling ramp.

To orient any domain structures present in the melt, the diblocks were flow-aligned at 160 °C using an aluminum channel die, shown schematically in Figure 1a, with the constraint (CD), flow (FD), and loading (LD) directions indicated. Prior to sample loading, the top and bottom surfaces of the die were coated with a thin layer of silicone oil (viscosity: 60 000 cSt

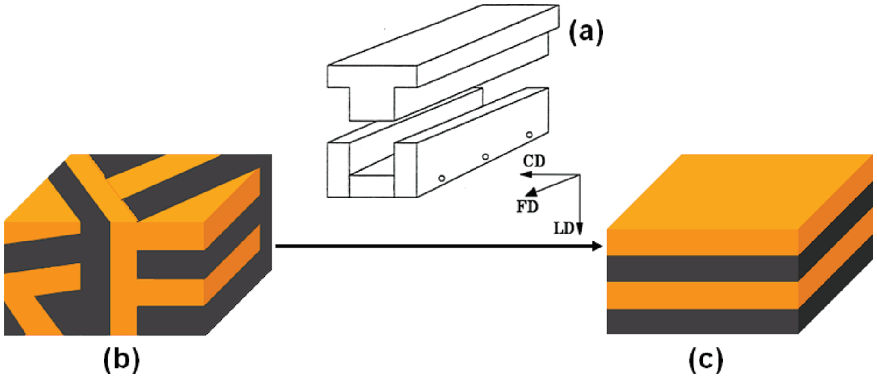

Figure 1. Schematic of channel-die flow alignment process. (a) Channel die schematic: CD is the constraint direction; FD is the flow direction; LD is the loading direction. (b) Unoriented lamella-forming block copolymer. (c) Channel-die-aligned block copolymer, with lamellar normals along LD.

at 23 °C). This fluid is immiscible with the block copolymers and has a much lower viscosity, such that when a compression force is applied along LD, most of the shear gradient occurs across the silicone oil layer, while the polymer itself undergoes nearly pure planar elongation.[37] If a block copolymer were to exhibit a lamellar domain structure, as would be expected for the high-octene diblocks based on their near-symmetric compositions ($f_{hard} \approx 0.5$), the flow field created by the channel die would tend to align the lamellae such that they lie down along FD, as illustrated schematically in Figure 1. The flow-aligned specimens were crystallized by quenching the entire die in a dry ice/isopropanol bath at −78 °C. Their solid-state morphologies and crystal orientations were examined using both static and time-resolved variable-temperature simultaneous small-angle (SAXS) and wide-angle X-ray scattering (WAXS) at the DuPont-Northwestern-Dow Collaborative Access Team (DND-CAT) beamline (5ID-D) at the Advanced Photon Source, Argonne National Laboratory. The X-ray energy was set at 10 keV (λ = 1.2398 Å). SAXS data were collected on a MAR USA CCD camera at a sample-to-detector distance of 8 m, while a quadrant of WAXS data was simultaneously collected on a Roper Scientific CCD camera at a sample-to-detector distance of either 140 or 227 mm. The use of this beamline was critical to this project because it allowed the acquisition of high-quality SAXS data at ultrasmall scattering angles. All X-ray scattering data were corrected for incident beam intensity, transmittance, and specimen thickness and so are presented on a consistent relative intensity scale.

For the variable-temperature X-ray experiments, the sample temperature was controlled using a Linkam DSC 600 hot stage. The channel-die-processed polymer strips were cut and stacked inside standard aluminum DSC pans (TA Instruments). To increase the transmittance, holes were punched through both the DSC pans and lids and covered with mica windows, 20 μm thick.[38] Three different temperature profiles were used in the time/temperature resolved experiments. Fast crystallization: heating from 20 to 150 °C at 20 °C/min, followed by 1 min hold at 150 °C, followed by cooling to 20 at 40 °C/min. Slow crystallization: heating from 20 to 150 °C at 20 °C/min, followed by 1 min hold at 150 °C, followed by cooling to 20 at 2 °C/min. Isothermal crystallization: heating from 20 to 150 °C at 20 °C/min, followed by 1 min hold at 150 °C, followed by quenching to a specified isothermal crystallization temperature, T_c, at 40 °C/min, followed by 15 min hold at T_c.

Results and Discussion

Crystallinity. The weight fraction crystallinity of the hard block, w_c, was calculated from the DSC-determined enthalpy, ΔH_m, using the equation

$$w_c = \frac{\Delta H_m}{f_{hard}\Delta H_m^0} \tag{3}$$

where ΔH_m^0 is the heat of fusion for 100% crystalline polyethylene (277 J/g).[39] The values of $T_{m,peak}$, $T_{c,onset}$, and w_c are summarized in Table 2. Equation 3 assumes that the soft block is fully amorphous, but for L52, two separate melting endotherms were observed during heating: a primary melting endotherm centered around $T_{m,peak}$ = 122 °C and a very shallow secondary melting endotherm (ΔH_m = 1.2 J/g) centered around $T \approx 50$ °C, attributed to the soft block.[40] Consequently, w_c for L52 was calculated based on ΔH_m for the primary melting endotherm alone. It is noteworthy that the measured $T_{m,peak}$ and w_c for the polyolefin diblocks are in excellent agreement with the values reported for ethylene−octene statistical copolymers, synthesized with single-site catalysts, having octene contents comparable to the hard blocks.[40,41]

χN Characterization. On the basis of the block copolymer molecular weight and composition data reported in Table 2, values of the number-average χN were estimated according to[42,43]

$$\chi N = \frac{M_n}{\rho RT}(\delta_{soft} - \delta_{hard})^2 \tag{4}$$

In eq 4, ρ is the block copolymer's mass density, estimated to be 0.77 g/cm^3 at 167 °C,[44,45] R is the gas constant; T is the absolute temperature, and δ_{soft} and δ_{hard} represent the solubility parameter for the soft and hard blocks, respectively. Reichart et al.[43] have measured δ for ethylene−octene (EO) copolymers, but out to only 54 wt % octene (23 mol % octene), so an extrapolation is required to obtain δ_{soft}. Their 167 °C data can be adequately correlated as

$$\delta_{EO} - \delta_{PE} = -(0.95\ \text{MPa}^{1/2})w_{oct} \tag{5}$$

where δ_{EO} is the solubility parameter of the EO copolymer containing a weight fraction octene equal to w_{oct}, δ_{PE} is the solubility parameter of linear ethylene homopolymer, and the standard error of the fitted coefficient is found to be 0.03 MPa$^{1/2}$. The correlation of eq 5 was used in eq 4 to calculate the χN values listed in Table 2. Note, however, that the choice of weight fraction (w_{oct}) as the correlating parameter in eq 5 is somewhat arbitrary; a similarly good linear fit can be obtained against mole fraction octene x_{oct}, which yields

$$\delta_{EO} - \delta_{PE} = -(2.41\ \text{MPa}^{1/2})x_{oct} \tag{6}$$

with the standard error of the fitted coefficient equal to 0.08 MPa$^{1/2}$. When extrapolated to the octene contents characteristic of the soft segments in the high-octene diblocks, eq 6 leads to lower values of δ_{soft} and correspondingly larger

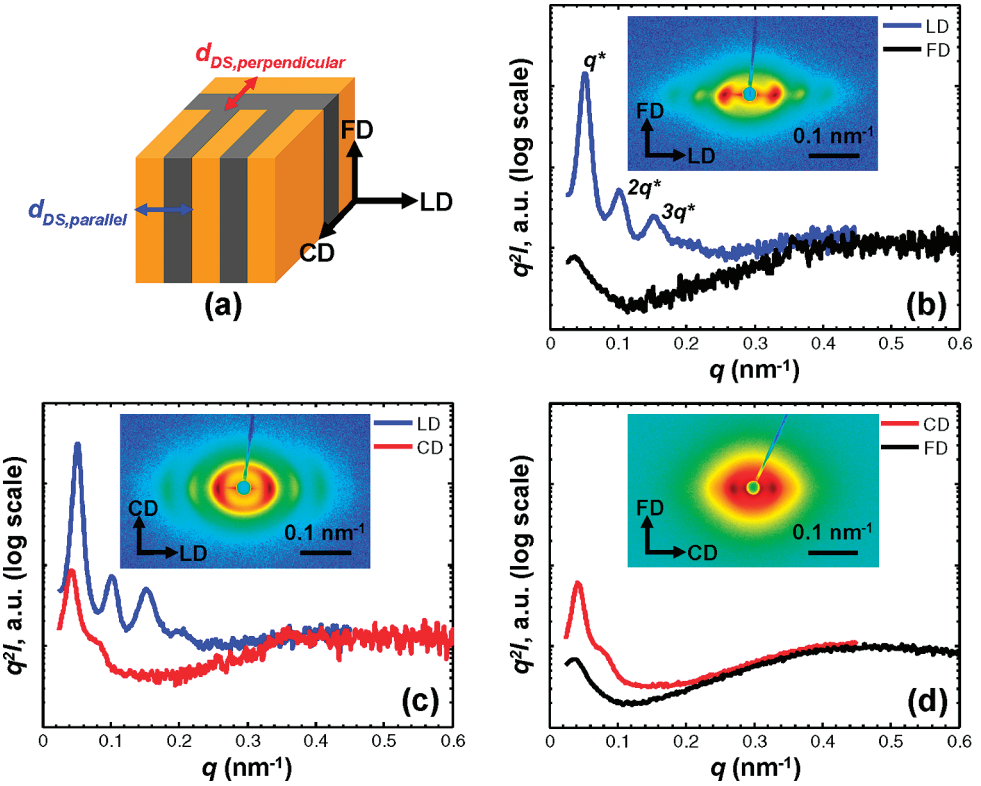

Figure 2. Room-temperature SAXS data for channel-die-aligned H69. (a) Schematic of lamellar domain structure after alignment. (b) CD-view SAXS data along LD (blue) and FD (black). (c) FD-view SAXS data along LD (blue) and CD (red). (d) LD-view SAXS data along CD (red) and FD (black). The insets in (b), (c), and (d) show the 2D SAXS patterns; the radial intensity profiles were obtained from the 2D patterns by averaging over a ±5° azimuthal band about the principal axis.

values of χ than does eq 5, by roughly a factor of 2 for the polymers considered here. This uncertainty in δ_{soft}, far more than any uncertainty in molecular weight, limits our accuracy in determining χN for these diblock copolymers.

For a monodisperse, linear diblock copolymer of symmetric composition, the order−disorder transition and critical point occur at a χN value of 10.5 in mean-field theory.[46] When the diblock copolymer is polydisperse, the χN value at the order−disorder transition is expected to decrease with increasing polydispersity;[23−25,27] a symmetric diblock copolymer wherein both blocks have the most-probable distribution, and with the lengths of the two blocks uncorrelated, should have a critical χN value of 4, where N is again calculated based on the number-average diblock length.[23] Comparing this critical χN to the χN values reported in Table 2 for our near-symmetric polydisperse ethylene−octene diblock copolymers, we expect the high-octene diblock copolymers to self-assemble into ordered structures in the melt, while L52 is likely to exhibit a homogeneous melt.

Melt and Solid-State Morphology. Having estimated the segregation strengths of the block copolymers, we proceeded to characterize their morphologies both in the melt and in the solid state. Typically, such a task is straightforward using X-ray techniques. However, direct determination of the melt morphology by SAXS is hampered by the near-zero X-ray contrast between the two polyolefin blocks in the melt; no SAXS intensity above background could be seen in any of the polymers in the melt, even with the excellent signal-to-noise ratio provided by the synchrotron beamline. Consequently, we probed these block copolymers' melt morphologies by an indirect method, which involved aligning the polymers in the melt and then crystallizing quiescently to preserve the oriented melt morphology for X-ray examination at room temperature, where there is strong X-ray contrast due to the different levels of crystallinity in the hard and soft domains.

The room-temperature 2D SAXS patterns for flow-aligned H69, taken with the X-ray beam parallel to CD, FD, and LD, are shown in Figure 2. The scattering patterns all show orientation anisotropy, with the highest scattering intensity concentrated along LD. This is consistent with H69 having an ordered morphology where the domains are predominantly aligned along FD, as depicted schematically in Figure 2a. To further probe the morphology, 1D intensity profiles were obtained along the three principal flow-alignment axes (i.e., FD, CD, and LD); the results are shown in Figure 2b−d. Each intensity profile was q^2-corrected to account for the appropriate form factor scattering,[47] where $q = (4\pi/\lambda) \sin \theta$, λ is the radiation wavelength and 2θ is the scattering angle. The SAXS reflections appear at integer ratios, where the first-, second-, and third-order reflections are clearly detectable. This suggests that H69 has a lamellar structure with well-defined long-range order, despite its large polydispersity. Its characteristic interlamellar domain spacing, d_{DS}, can be calculated from the position of the primary SAXS peak, q^*, via the following relation:

$$d_{DS} = \frac{2\pi}{q^*} \tag{7}$$

The parallel-type lamellae (lamellar normal parallel to LD) exhibit a q^* value of 0.0512 nm^{-1}; eq 7 thus yields $d_{DS} = 123$ nm. Polyethylene-based diblock copolymers of comparable average molecular weight but with near-monodisperse block lengths show domain spacings on the order of 50 nm.[18,48,49]

The much larger d-spacing exhibited by H69 is quite extraordinary and may be attributed to its polydispersity, as will be discussed further below. Besides the scattering from

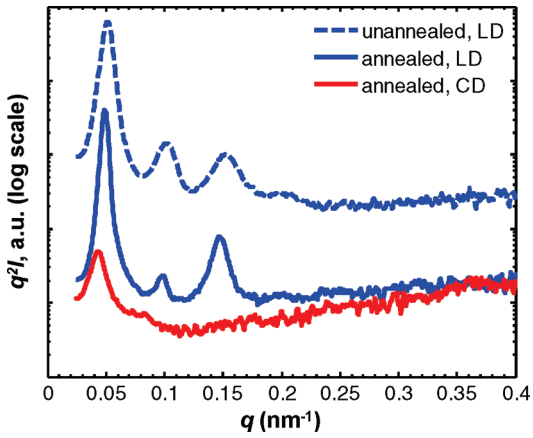

Figure 3. Room-temperature SAXS data for channel-die-aligned H69, beam parallel to FD. Solid lines represent data for the sample crystallized after annealing for 10 h in the melt, along LD (blue) and CD (red). Dashed blue line represents the intensity along LD for the unannealed sample, as in Figure 2c, shifted upward by a factor of 20 to avoid overlap.

the lamellar domains, the much broader scattering peak centered at $q \approx 0.5$ nm^{-1} is associated with scattering from the polyethylene crystallites.[4] The *d*-spacing of the crystallites, d_{cryst}, is ~13 nm, comparable to the intercrystallite repeat observed in hydrogenated anionically polymerized poly(high-1,4-butadiene),[4] which has a branch content (~4 mol % butene), melting temperature ($T_{m,peak} \approx$ 110 °C), and crystallinity ($w_c \approx 0.32$) all very similar to the hard block in these high-octene diblock copolymers.

A closer look at the 2D SAXS data in Figure 2 reveals that while the predominant orientation of the lamellar normals is along LD, there is a nonzero SAXS intensity along CD (in the FD and LD views, panels c and d, red curves) and even along FD (in the CD and LD views, panels b and d, black curves). While imperfect alignment in the simple channel die process is not atypical,[37] it is noteworthy that in H69 the *d*-spacings exhibited by the differently oriented lamellae are different, $d_{DS,parallel} = 123$ nm, while for the perpendicular-type lamellae (lamellar normal parallel to CD), $d_{DS,perpendicular} =$ 149 nm. This suggests that the lamellar structure has not reached equilibrium.

To assess this possibility, an aligned strip of H69 was annealed in the melt, outside of the channel die and unconstrained, in a vacuum oven at 160 °C for 10 h. The melt-annealed block copolymer was then recrystallized by removing it into ambient air. The FD-view SAXS pattern of the melt-annealed sample is qualitatively similar to that from the unannealed sample, as the orientation imposed on the block copolymer's melt structure is retained in the solid state; however, a few important differences are observable in the 1D data, as shown in Figure 3. First, annealing shifts the peak associated with the parallel lamellae to lower *q* (from 0.0512 to 0.0490 nm^{-1}), and the peak associated with the perpendicular lamellae to higher *q* (from 0.0423 to 0.0431 nm^{-1}), meaning that the differently oriented lamellae approach (but do not reach) a common spacing after 10 h of annealing. Second, the SAXS reflections sharpen; the full width at half-maximum of the primary SAXS peak associated with the (majority) parallel lamellae decreases from 0.0086 to 0.0055 nm^{-1}. Thus, the combination of channel die alignment and melt annealing transforms the defective lamellar structure which is initially present (as revealed in published transmission electron micrographs[21]) into a structure with excellent long-range order. Third, the relative intensities of the SAXS reflections change, with the second-order peak noticeably weaker after annealing.

The relative intensities of the peaks in a scattering profile are strongly influenced by the volume fractions of the dissimilar lamellae;[50] when the two types are of precisely equal thickness, the even-order peaks have identically zero intensity. Consequently, the decrease in second-order peak intensity following annealing might be interpreted, at first glance, as the result of a shift in the block copolymer's hard/soft domain volume fractions toward 50/50 upon annealing. However, since the polymer itself is nearly symmetric in composition, it is difficult to rationalize the initially asymmetric phase mixing which would be required to push the volume fractions away from 50/50. A more plausible explanation, consistent with the fact that the domain structure is not initially in equilibrium, is that the hard/soft domains are in fact close to the expected 50/50 ratio but that initially there are substantial local variations in the hard/soft volume fractions, thereby yielding a substantial intensity for the second-order peak. Annealing in the melt allows the material to approach its uniform, lowest-free-energy state, where the local composition (in addition to the domain spacing) is uniform throughout.

The fact that the parallel and perpendicular lamellae still exhibit different *d*-spacings after 10 h of annealing in the melt indicates that the polydisperse high-octene block copolymer H69 has an extraordinarily long structure equilibration time. This observation is in agreement with predictions made based on an extended strong segregation theory (SST) model, where the presence of polydispersity greatly reduces the free energy penalty for modest deviation from the equilibrium spacing.[21] More extensive discussion on the effect of polydispersity on block copolymer domain structure will be presented below.

To illustrate that the observed solid-state morphology of H69 is a replica of its melt structure, rather than reflecting structure developed during crystallization, we conducted time-resolved variable-temperature X-ray experiments on flow-aligned H69, following different crystallization histories: fast, slow, and isothermal. Representative SAXS data taken for H69 at different time/temperature points during the three different types of crystallization experiments are shown in Figure 4. Both the 2D images and the azimuthal intensity plots show that the channel-die-aligned lamellar orientation is preserved in all three experiments, even when crystallization is very slow; during isothermal crystallization at 93 °C, the crystallization half-time is ~6 min. Furthermore, all the SAXS data presented in Figure 4 were obtained from the same flow-aligned H69 specimen, via repeated heating and recrystallization (fast → isothermal → slow), and the lamellar orientation imparted by the channel die is retained through these heating/recrystallization cycles. These results confirm that the lamellar structure exhibited by H69 in the solid state is indeed a replica of the melt morphology and that the domain structures formed in the melt are extremely robust against distortion by crystallization.

Similar X-ray analyses were performed on the other polyolefin diblock copolymers. H81, H89, and H93 also displayed well-ordered lamellar morphologies regardless of the crystallization history employed, very similar to H69. Their respective interlamellar domain spacings, taken as the *d*-spacing displayed by the parallel lamellae after 10 h melt annealing, are listed in Table 2. As with H69, the domain spacings for perpendicular lamellae still exceeded those for parallel lamellae even after 10 h of melt annealing, but the difference was always less than 15%; we consider these

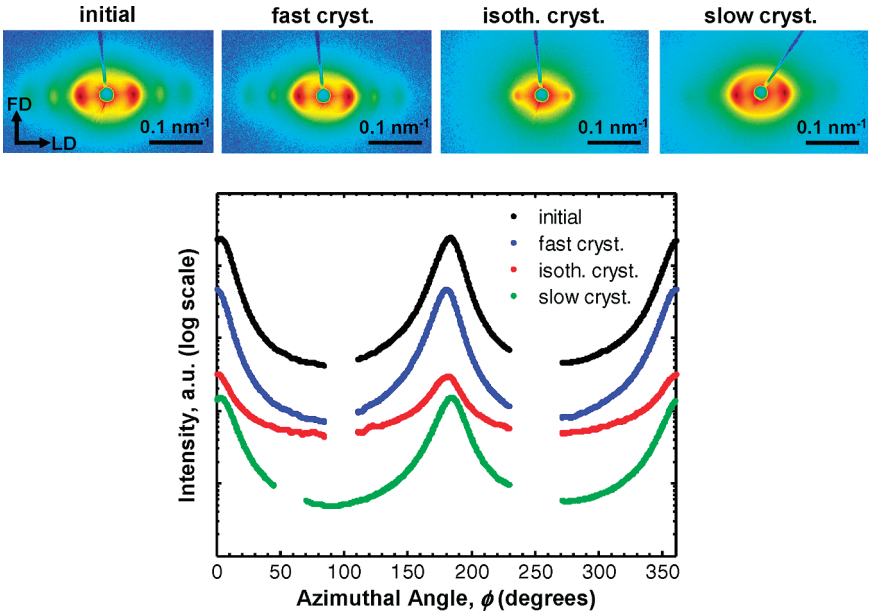

Figure 4. Top: CD-view SAXS patterns for H69 crystallized under different thermal histories. Bottom: corresponding azimuthal intensity profiles, averaged over the primary SAXS reflection (q = 0.03−0.06 nm^{-1}); ϕ = 0° and 180° denote LD; for clarity, azimuthal regions corresponding to the beamstop support and strong excess scattering from the DSC pan are removed, and the profiles are scaled by the following factors to avoid overlap: fast cryst., 0.2; isoth. cryst., 0.2; slow cryst., 0.01. "Initial" represents SAXS data acquired at T = 20 °C, prior to recrystallization; "fast cryst." represents SAXS data acquired at T = 20 °C, at the end of a fast crystallization experiment; "isoth. cryst." represents SAXS data acquired at the end of a 15 min isothermal crystallization at T_c = 93 °C; "slow cryst." represents SAXS data acquired at T = 20 °C, at the end of a slow crystallization experiment.

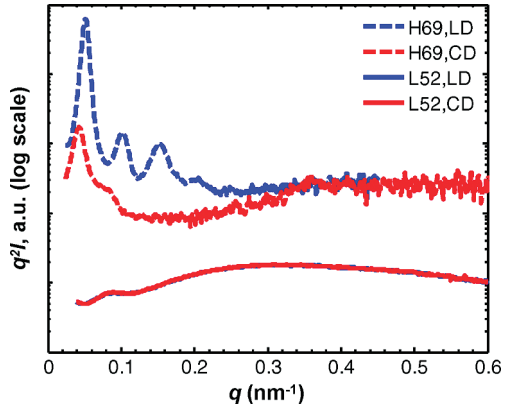

Figure 5. Solid curves: room-temperature SAXS data for low-octene diblock copolymer L52, beam parallel to FD. Intensity along LD shown in blue, along CD shown in red; the two curves completely overlap. For comparison, analogous data for H69 prior to melt-annealing (as in Figure 2c) are shown as dashed curves, shifted upward by a factor of 20 to avoid overlap.

values as a satisfactory approximation of the materials' equilibrium d-spacings.

In contrast to the high-octene diblock copolymers examined, L52 does not show any orientation in the solid state, as illustrated in Figure 5. This suggests that L52 has either a homogeneous melt with no domain structure to align or at most a weakly segregated melt whose structure is then destroyed in the process of crystallization, consistent with its small $\chi N \approx 2$.

Since the SAXS data for all four high-octene diblock copolymers indicate that crystallization proceeds within an ordered melt morphology, we initially expected to observe alignment of the crystals themselves.[16−19] When crystallization is confined inside lamellar domains, it has previously been shown that the crystal stems typically lie parallel to the lamellar interface, which orients both the fast-growth axis (for orthorhombic polyethylene, the b-axis) and the chain axis (c-axis) in the plane of the lamellae.[16,17] This simultaneously eliminates any requirement for commensurability between the crystallite spacing and the lamellar thickness and allows for unhindered growth of the crystals in their fast-growth direction. In Figure 6, the CD-view SAXS and WAXS data for H69 are both shown, following crystallization under either fast or isothermal conditions. Examination of the SAXS data (panel a) reveals only a small difference between the intensities of the "crystallite" peak ($q \approx 0.3$ nm^{-1} at 84 °C) along LD vs FD, indicating at most a very weak crystal orientation. The relevant WAXS data for the (110) and (200) reflections of the orthorhombic polyethylene crystal are shown in panel b. The azimuthal intensity profiles were normalized by the WAXS intensity in the melt at the same 2θ value, to correct for any apparent anisotropy due to nonuniform detector response or polarization effects. The absence of orientation in the polyethylene crystal unit cells is clearly evident.

The isothermal crystallization kinetics of the high-octene diblock copolymers were also investigated. At a given crystallization temperature, the relative polymer crystallinity at time t, $X_c(t)$, was determined from WAXS data by integrating the (110) and (200) peaks and normalized by the value at the end of the experiment (i.e., 15 min). The isothermal crystallization data thus obtained were then recast in the form of the Avrami equation:[51]

$$1 - X_c(t) = \exp(-kt^n) \tag{8}$$

The value of the Avrami exponent n often provides useful qualitative information on the nature of the crystallization process.[52] In the case of the polyolefin diblocks, as illustrated in Figure 7, n is found to be close to 3. This suggests highly interconnected crystal growth,[6,7,52] which is consistent with the lack of crystal orientation shown in Figure 6; though the lamellar domain structure is preserved, the lack of any crystal anisotropy in flow-aligned

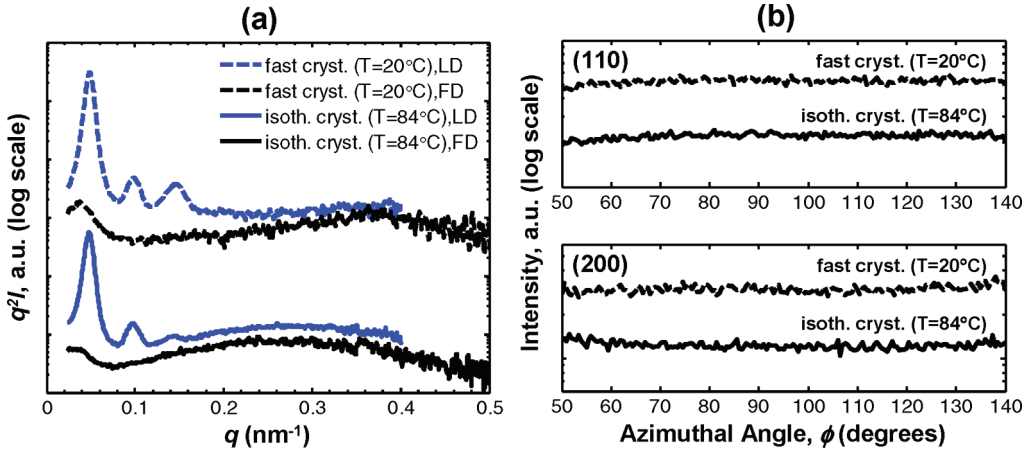

Figure 6. CD-view SAXS and WAXS data for channel-die aligned H69 crystallized under different thermal histories: cooling the melt to 20 at 40 °C/min ("fast cryst.", dashed lines) and isothermal crystallization at T_c = 84 °C for 15 min (solid lines). (a) SAXS intensity along LD (blue curves) and FD (black curves); "fast cryst." intensities are shifted upward by a factor of 200 to avoid overlap. (b) WAXS azimuthal intensities integrated over the angular range corresponding to the (110) and (200) peaks of orthorhombic polyethylene, respectively; ϕ = 0° and 180° denote LD; ϕ = 90° and 270° denote FD. In (b), the intensities have been normalized by the scattered intensities in the melt and scaled by the following factors for clarity: fast cryst. (110), 1.6; fast cryst. (200), 2.6.

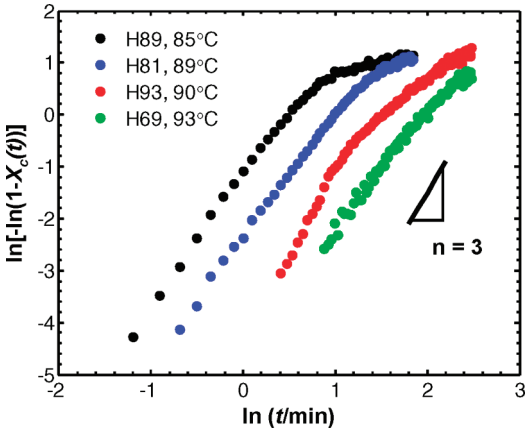

Figure 7. Avrami plot for isothermal crystallization of high-octene diblock copolymers.

specimens suggests that crystals can grow freely in all directions.

This combination—near-isotropic crystal growth for any crystallization conditions, with retention of the domain structure present in the melt—falls outside the breakout/templated/confined scheme[7,53] which effectively classifies more conventional near-monodisperse block copolymers. We believe that this surprising crystallization behavior in these high-octene olefin block copolymers is a result of soft/hard block phase mixing: specifically, the dissolution of short hard blocks in the soft domain. Because of the polydisperse nature of our polymers, the hard and soft blocks in any given chain may be greatly mismatched in length. When this mismatch is sufficiently large, the shorter block may be pulled away from the domain interface and dissolved in the domains rich in the unlike block.[26] Such phase mixing, which will be elaborated further below, could then lead to isotropic crystal orientation in the solid state, since the hard blocks dissolved in the soft domains can still crystallize upon cooling: a crystal nucleated in a hard-block-rich domain need not stop growing when it reaches the lamellar interface but instead may continue to grow through the soft domain via the dissolved hard blocks, without requiring the transport of blocks between domains. Indeed, the fact that w_c for the hard blocks (Table 2) is similar to that for statistical copolymers of the same octene content[40] indicates that these dissolved hard blocks must crystallize to a similar extent as those in the hard-block-rich domains. Consequently, even though the lamellar structure is preserved upon crystallization, it exerts no "templating" or "confining" effect on the growing crystals, leading to a new mode of crystallization within heterogeneous block copolymers, which we term "pass through".

Effect of Polydispersity on Domain Periodicity. Despite being highly polydisperse, each of the four high-octene diblock copolymers exhibits a lamellar melt morphology with good long-range order, in agreement with other recent studies on polydisperse block copolymers. Bendejacq et al. investigated several polydisperse poly(styrene)-*b*-poly(acrylic acid) diblock copolymers, synthesized by controlled radical polymerization,[54] and concluded that despite the broad molecular weight distributions, they exhibited well-ordered cylindrical and lamellar morphologies. In a systematic investigation by Lynd et al. on poly(ethylene-*alt*-propylene)-*b*-poly(DL-lactide) diblocks, where the PDI of the poly(DL-lactide) block was varied, the copolymers also formed well-ordered domain structures; changes in the poly(DL-lactide) block PDI had negligible influence on the regularity of the domain lattice.[32]

Although polydispersity may not impede the self-assembly of block copolymers into regular domain lattices, its influence on other aspects of block copolymer phase behavior can be significant indeed.[22] According to theory, increasing polydispersity at fixed M_n increases the domain periodicity.[24−26] In a polydisperse block copolymer, the chains can fill space most effectively by having the longer ones occupy the centers of the domains, while the shorter ones are concentrated at the interfaces. This arrangement alleviates the entropy cost associated with chain stretching, resulting in a larger equilibrium spacing.[24−26] In addition to chain stretching, block copolymer domain spacing is further increased due to phase mixing,[26] as discussed previously; chain pull-out is entropically favorable since it frees the block junctions from being anchored at the interfaces. The impact of phase mixing on block copolymer domain swelling is expected to be most important at small values of χN, where the enthalpic cost of mixing dissimilar blocks is small.

To assess the effect of polydispersity on domain spacing, the spacings for the high-octene diblocks are plotted as a function of molecular weight in Figure 8, along with values

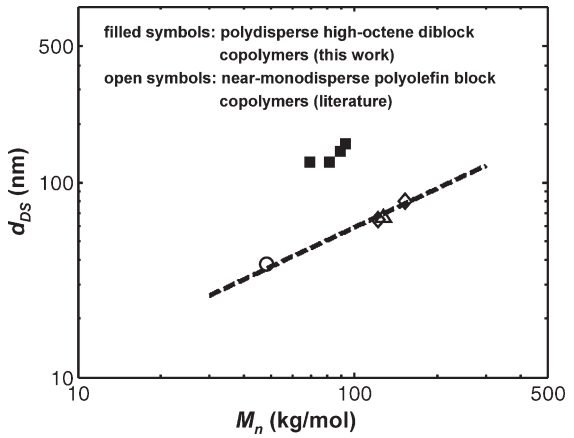

Figure 8. Block copolymer domain spacing (d_{DS}) as a function of molecular weight (M_n). Filled squares represent the polydisperse high-octene diblock copolymers reported herein, where each block ideally has a most probable distribution. Open symbols represent literature data for near-monodisperse lamella-forming polyethylene-containing polyolefin block copolymers: poly(ethylene)-*b*-poly(head-to-head propylene) (open circle),[48] poly(ethylene)-*b*-poly(ethylene-*alt*-propylene) (open triangle),[18] and poly(ethylene)-*b*-poly(ethylene-*alt*-propylene)-*b*-poly(ethylene) triblocks (open diamonds);[49] for the triblocks, M_n is taken as $M_{n,triblock}/2$. Dashed line drawn through the near-monodisperse data has the form $d_{DS} \propto M_n^{2/3}$.

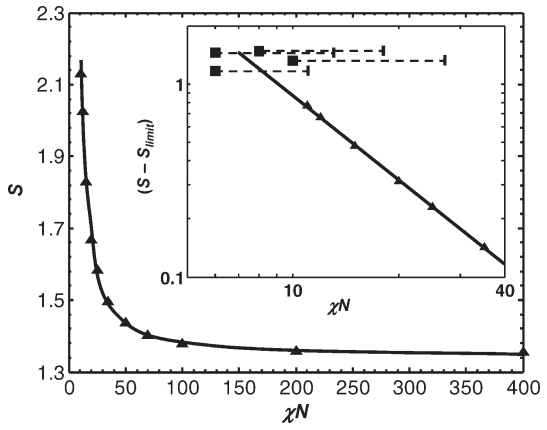

Figure 9. Self-consistent-field theory (SCFT) predictions for the relative degree of domain swelling (S) in lamella-forming diblock copolymers with the most probable distribution in both blocks, and no correlation between block lengths, as a function of segregation strength (χN). The continuous curve is simply a guide for the eye. In addition to previously published[26] values of S at selected values of χN, this plot includes additional unpublished values calculated by Matsen via the same methodology, including several for $\chi N < 25$, the region of principal interest in this work. Inset focuses on the region of small χN, and the experimental results for the polydisperse high-octene diblocks are included for comparison. In the inset, the y-axis is presented as $S - S_{limit}$, where S_{limit} ($\approx$1.352) is the limiting extent of swelling at asymptotically strong segregation; the solid line is the best fit to the SCFT predictions for $\chi N \leq 50$. Squares represent the experimental data with χN calculated by a weight-fraction extrapolation of the solubility parameter data (eq 5), while the vertical bars (connected to the squares by dashed lines) represent the experimental data with χN calculated by a mole fraction extrapolation (eq 6).

reported for several monodisperse polyethylene-based block copolymers[18,48,49] having molecular weights and chemical structures similar to those of our olefin diblock copolymers and generally similar solubility parameters for the amorphous block[42,55] (hence similar χ). As illustrated in Figure 8, at a given block copolymer molecular weight, raising the PDI from 1 to 2 increases the domain spacing by a factor of $\sim$2.7. The dashed line passing through the monodisperse data has the form[56]

$$d_{DS} \propto M_n^{2/3} \tag{9}$$

Such a scaling relationship is well-established for monodisperse block copolymers in the strong segregation limit, and as shown in Figure 8, it describes the reported monodisperse data well. No attempt was made to fit a scaling law to the polydisperse data; besides the limited range of M_n in Figure 8, the four polydisperse high-octene diblock copolymers have somewhat different octene contents, so both the statistical segment length and χ vary moderately across the series, and each of these quantities also influences the domain periodicity.[56] (Parenthetically, the same is true for the monodisperse data, since the comparison includes polymers where the amorphous block is either poly(ethylene-*alt*-propylene) or head-to-head polypropylene, yet a common scaling adequately represents both cases.) Fortunately, the solubility parameters of the two amorphous polymers used in the monodisperse data are similar in magnitude[55] to the values calculated for the soft blocks in our ethylene−octene diblocks by eqs 5 and 6, so variations in χ do not greatly complicate the comparison in Figure 8.

The observed increase in domain spacing with increasing PDI is in qualitative agreement with previously reported computational and experimental results. Recently, Matsen used self-consistent-field theory (SCFT) to investigate the effects of polydispersity on block copolymer morphology.[26] He reported the relative degree of domain swelling, $S = d_{DS,polydisperse}/d_{DS,monodisperse}$, for diblock copolymers following the Zimm−Schulz distribution, with varying PDI and block segregation strength; the results for lamella-forming diblock copolymers with PDI = 2 in both blocks and varying χN are reproduced in Figure 9, including several additional results provided by Matsen in addition to those previously published,[26] extending down to $\chi N = 11$ (recall that the monodisperse case whose domain spacing forms the denominator in S is disordered for $\chi N < 10.5$). As expected, the degree of domain swelling is most severe at small χN, where component mixing is extensive; i.e., a significant fraction of the block junctions are not localized at the domain interfaces. These calculations also showed that such swelling effects persist into the strong segregation limit and asymptotically approach a limiting value, S_{limit}, which for the system presented in Figure 9 occurs at $S_{limit} \approx 1.352$; the asymptotic $S_{limit} > 1$ reflects solely the reduction in stretching energy due to polydispersity, as in this asymptotic limit, all block junctions are localized at interfaces. The inset of Figure 9 shows the same set of domain swelling predictions but focuses on the region of small χN and subtracts S_{limit} to highlight the influence of intercomponent mixing on S. In the inset, we also include the experimental results for the polydisperse high-octene diblock copolymers; in the calculation of S, $d_{DS,monodisperse}$ was obtained from the 2/3 power fit to the literature data shown in Figure 8, while χN was calculated with the correlation in eq 5. The experimental values of S are similar in magnitude to a straightforward extrapolation of the SCFT calculations, providing further support to the idea that there is extensive intercomponent mixing in these block copolymers. In fact, if χN is calculated instead by a mole fraction extrapolation of solubility parameters (eq 6), this yields the short vertical bars in Figure 9; these lie substantially above the SCFT calculations, implying an even greater degree of domain swelling than predicted by SCFT. Unfortunately, a detailed comparison of experiment and theory is hampered by the uncertainty in χ associated with extrapolating the available solubility parameter data.

While the most notable difference between our polymers and the near-monodisperse materials whose domain spacings are reported in Figure 8 is in fact the polydispersity, we considered to what extent the domain spacing might be influenced by other dissimilarities between the materials. First, the monodisperse block copolymers in Figure 8 contain less mass in their side groups (i.e., methyl vs hexyl). Since the comparison is made at equivalent M_n, putting a larger fraction of the mass into the side groups should *decrease* the domain spacing, contrary to our observations. Though the exact magnitude of this effect depends on the detailed conformational statistics of the blocks, its direction is clear: monodisperse analogues of our ethylene−octene diblocks should show domain spacings even smaller than the "literature" values in Figure 8.

Another factor that may influence the domain swelling ratio is that the olefin diblock copolymers studied in this work contain "free" hard and soft blocks as impurities—chains which are not part of a diblock copolymer, formed by chain transfer during polymerization. Ideally, all polymer chains exiting the reactor train should be bound to a Zn atom, two chains per Zn (from the diethylzinc CSA).[20] But comparison of the Zn content measured by X-ray fluorescence in the high-octene polymers with their M_n values in Table 2 indicates 2.8−3.2 chains per Zn in the product; this translates to a free chain content of roughly 20 wt %, if the free chains have the same average molecular weight as one of the blocks in the symmetric diblock. The presence of free chains is also evident in the PDI values in Table 2: for a symmetric polymer wherein both blocks have the most-probable distribution, the PDI should ideally equal 1.5,[20] but the observed values are ∼2. Comparison with L52, which shows a lower PDI, suggests that chain transfer becomes more significant at higher molecular weights and/or octene contents. The presence of essentially free soft segment in the high-octene diblocks was confirmed by room-temperature solvent extraction. When the as-received diblock copolymer pellets were stirred with *n*-hexane at room temperature for 10 days, 10−15 wt % of a polymeric material was extracted. This extracted material was amorphous as determined by DSC, and it had an ethylene/octene ratio near that expected for the soft block in the diblocks, based on the reactor operating conditions and a preliminary assessment of the soft-block octene content in the whole polymer by ^{13}C NMR.

The presence of free chains leads to overestimation of the degree of domain swelling in two ways. First, the presence of homopolymer chains with molecular weights comparable to that of the corresponding block chain is known to cause domain swelling in block copolymers.[57−60] On the basis of the results of Torikai et al. on AB/A/B ternary blends of near-monodisperse components, where A is polystyrene and B is poly(2-vinylpyridine), the presence of 20 vol % homopolymer (10 vol % A, 10 vol % B, each of comparable molecular weight to the analogous block in the AB diblock) leads to a 20% increase in domain spacing.[60] Second, the molecular weights reported in Table 2 correspond to whole polymer samples, containing both diblock and free chains, and are thus underestimates of the true diblock M_n. On the basis of the blend M_n values and the estimated free chain contents, the true diblock M_n should be about 25% higher than the values in Table 2. With a $d_{DS} \propto M_n^{2/3}$ scaling, this effect could translate to a 16% reduction in domain swelling ratio, bringing the polydisperse and monodisperse data in Figure 8 slightly closer together, but not by nearly enough to close the gap. In short, while the comparison in Figure 8 is not perfect, it is clear that the influence of factors other than polydispersity on the domain spacing is small by comparison.

Conclusions

Near-symmetric polydisperse olefin diblock copolymers, with an octene differential between the soft and hard blocks exceeding 25 mol % and number-average molecular weights of 69−93 kg/mol, self-assembled in the melt into well-ordered lamellar structures with domain spacings well above 100 nm. These lamellar domains exhibited an extraordinarily long structural equilibration time, exceeding 10 h. The lamellar structures were also preserved in the solid state, with no significant dependence on crystallization history. However, the resulting crystals were isotropic in orientation, even when the block copolymer lamellae were highly aligned. All polymers showed crystallization kinetics with an Avrami exponent $n \approx 3$, indicating interconnected crystal growth, which traverses the domain interfaces. Dissolution of short hard blocks in the soft domains, facilitated by these materials' large polydispersities, allowed crystals to grow through both the hard and soft domains without destroying the interfaces established in the melt.

Comparing the lamellar domain spacings of these polydisperse high-octene diblock copolymers to those of monodisperse block copolymers with similar molecular weight and chemical structure, we observed a nearly 3-fold increase in periodicity. Such a large extent of domain swelling reflects the high polydispersity in both blocks (most-probable distribution) and the modest segregation strength in these materials, such that short blocks of either type are largely dissolved in domains rich in blocks of the other type. These results indicate that controlled polydispersity in both blocks offers a route to generating lamellar domain structures with an exceptionally large period, while preserving the long-range order commonly associated with near-monodisperse block copolymers.

Acknowledgment. This work was supported by the Dow Chemical Company and the National Science Foundation, Polymers Program (DMR-0505940 and DMR-1003942). The X-ray experiments were performed at the DuPont-Northwestern-Dow Collaborative Access Team (DND-CAT) beamline, located at Sector 5 of the Advanced Photon Source (APS). DND-CAT is supported by E.I. DuPont de Nemours & Co., The Dow Chemical Company, and the State of Illinois. Use of the APS was supported by the U.S. Department of Energy, Office of Science, Office of Basic Energy Sciences, under Contract DE-AC02-06CH11357. The authors gratefully acknowledge Mark Matsen (University of Reading) for the SCFT calculations whose results are presented in Figure 9 and for his interest in this work. The authors also thank Gary Marchand and Patricia Roberts (Dow Chemical) for stimulating discussions throughout.

References and Notes

(1) Hamley, I. W. *Adv. Polym. Sci.* **1999**, *148*, 113–137.
(2) Loo, Y. L.; Register, R. A. Crystallization Within Block Copolymer Mesophases. In *Development in Block Copolymer Science and Technology*; Hamley, I. W., Ed.; John Wiley & Sons, LTD: Chichester, 2004; pp 213−243.
(3) Muller, A. J.; Balsamo, V.; Arnal, M. L. *Adv. Polym. Sci.* **2005**, *190*, 1–63.
(4) Rangarajan, P.; Register, R. A.; Fetters, L. J. *Macromolecules* **1993**, *26*, 4640–4645.
(5) Lee, L. B. W.; Register, R. A. *Macromolecules* **2004**, *37*, 7278–7284.
(6) Loo, Y. L.; Register, R. A.; Ryan, A. J.; Dee, G. T. *Macromolecules* **2001**, *34*, 8968–8977.
(7) Loo, Y. L.; Register, R. A.; Ryan, A. J. *Macromolecules* **2002**, *35*, 2365–2374.
(8) Nojima, S.; Kato, K.; Yamamoto, S.; Ashida, T. *Macromolecules* **1992**, *25*, 2237–2242.
(9) Nojima, S.; Nakano, H.; Ashida, T. *Polymer* **1993**, *34*, 4168–4170.
(10) Nojima, S.; Nakano, H.; Takahashi, Y.; Ashida, T. *Polymer* **1994**, *35*, 3479–3486.

(11) Rangarajan, P.; Register, R. A.; Adamson, D. H.; Fetters, L. J.; Bras, W.; Naylor, S.; Ryan, A. J. *Macromolecules* **1995**, *28*, 1422–1428.
(12) Loo, Y. L.; Register, R. A.; Ryan, A. J. *Phys. Rev. Lett.* **2000**, *84*, 4120–4123.
(13) Quiram, D. J.; Register, R. A.; Marchand, G. R. *Macromolecules* **1997**, *30*, 4551–4558.
(14) Quiram, D. J.; Register, R. A.; Marchand, G. R.; Ryan, A. J. *Macromolecules* **1997**, *30*, 8338–8343.
(15) Shiomi, T.; Takeshita, H.; Kawaguchi, H.; Nagai, M.; Takenaka, K.; Miya, M. *Macromolecules* **2002**, *35*, 8056–8065.
(16) Douzinas, K. C.; Cohen, R. E. *Macromolecules* **1992**, *25*, 5030–5035.
(17) Cohen, R. E.; Bellare, A.; Drzewinski, M. A. *Macromolecules* **1994**, *27*, 2321–2323.
(18) Hamley, I. W.; Fairclough, J. P. A.; Terrill, N. J.; Ryan, A. J.; Lipic, P. M.; Bates, F. S.; Towns-Andrews, E. *Macromolecules* **1996**, *29*, 8835–8843.
(19) Zhu, L.; Cheng, S. Z. D.; Calhoun, B. H.; Ge, Q.; Quirk, R. P.; Thomas, E. L.; Hsiao, B. S.; Yeh, F. J.; Lotz, B. *J. Am. Chem. Soc.* **2000**, *122*, 5957–5967.
(20) Hustad, P. D.; Kuhlman, R. L.; Arriola, D. J.; Carnahan, E. M.; Wenzel, T. T. *Macromolecules* **2007**, *40*, 7061–7064.
(21) Hustad, P. D.; Marchand, G. R.; Garcia-Meitin, E. I.; Roberts, P. L.; Weinhold, J. D. *Macromolecules* **2009**, *42*, 3788–3794.
(22) Lynd, N. A.; Meuler, A. J.; Hillmyer, M. A. *Prog. Polym. Sci.* **2008**, *33*, 875–893.
(23) Burger, C.; Ruland, W.; Semenov, A. N. *Macromolecules* **1990**, *23*, 3339–3346.
(24) Sides, S. W.; Fredrickson, G. H. *J. Chem. Phys.* **2004**, *121*, 4974–4986.
(25) Cooke, D. M.; Shi, A. C. *Macromolecules* **2006**, *39*, 6661–6671.
(26) Matsen, M. W. *Eur. Phys. J. E* **2006**, *21*, 199–207.
(27) Matsen, M. W. *Phys. Rev. Lett.* **2007**, *99*, 148304.
(28) Matsushita, Y.; Noro, A.; Iinuma, M.; Suzuki, J.; Ohtani, H.; Takano, A. *Macromolecules* **2003**, *36*, 8074–8077.
(29) Noro, A.; Iinuma, M.; Suzuki, J.; Takano, A.; Matsushita, Y. *Macromolecules* **2004**, *37*, 3804–3808.
(30) Noro, A.; Cho, D.; Takano, A.; Matsushita, Y. *Macromolecules* **2005**, *38*, 4371–4376.
(31) Lynd, N. A.; Hillmyer, M. A. *Macromolecules* **2005**, *38*, 8803–8810.
(32) Lynd, N. A.; Hamilton, B. D.; Hillmyer, M. A. *J. Polym. Sci., Part B: Polym. Phys.* **2007**, *45*, 3386–3393.
(33) Lynd, N. A.; Hillmyer, M. A. *Macromolecules* **2007**, *40*, 8050–8055.
(34) Meuler, A. J.; Ellison, C. J.; Hillmyer, M. A.; Bates, F. S. *Macromolecules* **2008**, *41*, 6272–6275.
(35) Chang, F. S. C. *J. Chromatogr.* **1971**, *55*, 67–71.
(36) Sebastian, J. M.; Register, R. A. *J. Appl. Polym. Sci.* **2001**, *82*, 2056–2069.
(37) Lee, H. H.; Register, R. A.; Hajduk, D. A.; Gruner, S. M. *Polym. Eng. Sci.* **1996**, *36*, 1414–1424.
(38) Ryan, A. J. *J. Therm. Anal.* **1993**, *40*, 887–899.
(39) Brandrup, J., Immergut, E. H., Eds.; *Polymer Handbook*, 3rd ed.; Wiley: New York, 1989.
(40) Chen, H. Y.; Chum, S. P.; Hiltner, A.; Baer, E. *J. Polym. Sci., Part B: Polym. Phys.* **2001**, *39*, 1578–1593.
(41) Kim, M. H.; Phillips, P. J. *J. Appl. Polym. Sci.* **1998**, *70*, 1893–1905.
(42) Graessley, W. W.; Krishnamoorti, R.; Balsara, N. P.; Butera, R. J.; Fetters, L. J.; Lohse, D. J.; Schulz, D. N.; Sissano, J. A. *Macromolecules* **1994**, *27*, 3896–3901.
(43) Reichart, G. C.; Graessley, W. M.; Register, R. A.; Lohse, D. J. *Macromolecules* **1998**, *31*, 7886–7894.
(44) Fetters, L. J.; Lohse, D. J.; Richter, D.; Witten, T. A.; Zirkel, A. *Macromolecules* **1994**, *27*, 4639–4647.
(45) Han, S. J.; Lohse, D. J.; Condo, P. D.; Sperling, L. H. *J. Polym. Sci., Part B: Polym. Phys.* **1999**, *37*, 2835–2844.
(46) Leibler, L. *Macromolecules* **1980**, *13*, 1602–1617.
(47) Shibayama, M.; Hashimoto, T. *Macromolecules* **1986**, *19*, 740–749.
(48) Rangarajan, P.; Register, R. A.; Fetters, L. J.; Bras, W.; Naylor, S.; Ryan, A. J. *Macromolecules* **1995**, *28*, 4932–4938.
(49) Koo, C. M.; Wu, L. F.; Lim, L. S.; Mahanthappa, M. K.; Hillmyer, M. A.; Bates, F. S. *Macromolecules* **2005**, *38*, 6090–6098.
(50) Hashimoto, T.; Nagatoshi, K.; Todo, A.; Hasegawa, H.; Kawai, H. *Macromolecules* **1974**, *7*, 364–373.
(51) Avrami, M. *J. Chem. Phys.* **1939**, *7*, 1103–1112.
(52) Mandelkern, L. *Crystallization of Polymers*; McGraw-Hill: New York, 1964.
(53) Xu, J. T.; Fairclough, J. P. A.; Mai, S. M.; Ryan, A. J.; Chaibundit, C. *Macromolecules* **2002**, *35*, 6937–6945.
(54) Bendejacq, D.; Ponsinet, V.; Joanicot, M.; Loo, Y. L.; Register, R. A. *Macromolecules* **2002**, *35*, 6645–6649.
(55) Graessley, W. W.; Krishnamoorti, R.; Reichart, G. C.; Balsara, N. P.; Fetters, L. J.; Lohse, D. J. *Macromolecules* **1995**, *28*, 1260–1270.
(56) Bates, F. S.; Fredrickson, G. H. *Annu. Rev. Phys. Chem.* **1990**, *41*, 525–557.
(57) Tanaka, H.; Hasegawa, H.; Hashimoto, T. *Macromolecules* **1991**, *24*, 240–251.
(58) Hashimoto, T.; Tanaka, H.; Hasegawa, H. *Macromolecules* **1990**, *23*, 4378–4386.
(59) Winey, K. I.; Thomas, E. L.; Fetters, L. J. *Macromolecules* **1991**, *24*, 6182–6188.
(60) Torikai, N.; Takabayashi, N.; Noda, I.; Koizumi, S.; Morii, Y.; Matsushita, Y. *Macromolecules* **1997**, *30*, 5698–5703.